Three-wave interaction solitons in optical parametric amplification

E. Ibragimov* and A. A. Struthers†
Department of Mathematical Sciences, Michigan Technological University, Houghton, Michigan 49931-1295

D. J. Kaup‡
Institute of Nonlinear Studies and Department of Mathematics and Physics, Clarkson University, Potsdam, New York 13699-5815

J. D. Khaydarov
Continuum Incorporated, Santa Clara, California 95091

K. D. Singer
Department of Physics, Case Western Reserve University, Cleveland, Ohio 44106
(Received 1 July 1998; revised manuscript received 5 January 1999)

This paper applies three-wave interaction (TWI)-soliton theory to optical parametric amplification when the signal, idler, and pump wave can all contain TWI solitons. We use an analogy between two different velocity regimes to compare the theory with output from an experimental synchronously pumped optical parametric amplifier. The theory explains the observed inability to compress the intermediate group-velocity wave and 20-fold pulse compression in this experiment. The theory and supporting numerics show that one can effectively control the shape and energy of the optical pulses by shifting the TWI solitons in the pulses. [S1063-651X(99)16505-X]

PACS number(s): 42.65.Tg, 42.65.Yj, 42.65.Re, 42.65.Ky

I. INTRODUCTION

To adequately describe three-wave interactions (TWI's) involving ultrashort laser pulses ($\tau \leqslant 10$ ps), it is necessary to account for dispersive effects. Normally, such effects limit conversion efficiency and elongate pulses in second harmonic generation (SHG), sum frequency generation (SFG), optical parametric generation (OPG), and optical parametric amplification processes. However, as early as in 1968 [1] it was shown that in optical parametric amplification due to the group-velocity mismatch, the fundamental wave can be substantially compressed in a degenerate interaction (when the group velocities of the two fundamentals are equal). More recently it was predicted theoretically [2,3] and observed experimentally [4,5] that group-velocity mismatch (GVM) can compress ultrashort laser pulses in SHG and SFG processes. In recent experiments pulse compression ascribed to GVM was also observed in OPG and OPA experiments [6–9]. That this compression was soliton in nature, as originally proposed in Ref. [3], had until very recently not been given adequate consideration.

In Refs. [10,11] the soliton nature of pulse compression in the presence of the GVM was explained using analytical soliton solutions [12,13] derived from the inverse scattering transform (IST): extensions of these soliton solutions to nonzero phase mismatch were contained in [11], where these solitons were termed TWI-solitons to distinguish them from other more familiar solitons. TWI solitons, although they exist in quadratic $\chi^{(2)}$ media, differ greatly from the well-known solitary waves generated by cascading $\chi^{(2)} \times \chi^{(2)}$ processes [14,15]. Unlike the cascaded waves, TWI solitons are not a composition of two waves with different frequencies and oscillatory profiles moving together. In contrast, TWI solitons are single frequency pulses with smooth, for a single TWI-soliton sech, profiles. Moreover, TWI solitons do not require high second-order group-velocity dispersion (GVD) and are supported entirely by the first-order group-velocity mismatch effect. This feature makes TWI solitons especially attractive for applications in all optical switching [16].

The underlying scattering problem (developed in Refs. [12,13], and summarized in Ref. [17]) for the TWI system is the unwieldy third order Zahkarov-Manakov (ZM) system of differential equations. Fortunately, when the pulses do not overlap the ZM system factors into three simpler Zahkarov-Shabat (ZS) scattering problems: the ZS scattering problem underlies the nonlinear Schrödinger equation (NLS) soliton theory, and has been intensively studied because of important applications in optical data transmission.

The IST theory shows a connection between the scattering problem for the NLS system and the asymptotic scattering problems for the TWI system. A connection between the TWI system and NLS equation is not surprising. As early as 1976 the authors of [18] noted solitonlike propagation of optical pulses in quadratic media. These phenomena are the subject of recent intense theoretical and experimental [14,15] investigation. The connection between the ZM scattering problem and three ZS scattering problems (one for the asymptotic profile of each frequency) shows that we should expect profiles similar to those seen in the NLS as output from the three-wave interaction. However, one must remember that, although the inverse scattering problems are the same for the NLS and the asymptotics for each frequency in

*Electronic address: ibragimo@engr.umbc.edu Present address: Electrical Engineering, University of Maryland, Baltimore County, Baltimore, MD 21250.
†Electronic address: struther@mtu.edu
‡Electronic address: kaup@sun.mcs.clarkson.edu

TWI, the temporal propagation equations are, of course, completely different.

In this paper we present results obtained using IST tools, describing pulse compression effects in optical parametric amplification: it appears that IST theory provides an explanation of a substantial body of experimental data accumulated over the last few years in optical parametric generation and optical harmonic generation by ultrashort laser pulses. Specifically, we explain the experimentally measured 20-fold compression [6,7] of the idler wave in a synchronously pumped optical parametric generator, and note the successful explanation [19] of the compression reported in these works.

II. BASIC PROPERTIES OF TWI SOLITONS

A numerical study in Ref. [11] shows that group velocity dispersion is negligible in most practical cases and we neglect GVD effects. In this regime the three-wave interaction is described by the following system of three equations:

$$\frac{\partial A_1}{\partial z}+\frac{1}{v_1}\frac{\partial A_1}{\partial t}=A_3A_2,$$

$$\frac{\partial A_2}{\partial z}+\frac{1}{v_2}\frac{\partial A_2}{\partial t}=A_3A_1, \tag{1}$$

$$\frac{\partial A_3}{\partial z}+\frac{1}{v_3}\frac{\partial A_3}{\partial t}=-A_1A_2,$$

where A_j are normalized amplitudes: $A_j=(E_j/E_0)\sqrt{n_j\omega_3/n_3\omega_j}$, ω_j are frequencies, v_j are group velocities, and n_j are the refractive indexes. E_0 here is determined by the relationship $E_0=\sqrt{n_1n_2\lambda_1\lambda_2}/(2\pi)^2\chi_{nl}$, where χ_{nl} is the nonlinear dielectric susceptibility.

Throughout this paper we assume perfect phase matching, i.e., $\Delta k=0$. This assumption is not necessary for the analysis in the paper, and is adopted for simplicity and clarity: we can use the phase transformation in [11] to connect system (1) to the analogous system with $\Delta k\neq 0$.

We assume that the group velocity of the high frequency wave, v_3, lies between the group velocities of the other two waves, i.e., $v_1>v_3>v_2$. In Ref. [16] this is the FSF (fundamental–sum frequency–fundamental) case. In Ref. [17] this is the ''soliton-decay'' case. In the FSF regime both fundamental frequencies can contain TWI solitons. In contrast, if the group velocity v_3 of the pump does not lie between the fundamental group velocities v_1 and v_2—we term this the SFF (sum frequency–fundamental–fundamental) regime—only the fundamental frequency with the extreme velocity can have TWI solitons. As shown below, this distinction between the two regimes plays an important role when comparing the TWI soliton theory and experimental data. Throughout this paper we use FSF soliton theory: in Sec. IV we show how this theory can be applied to an experimental SFF interaction.

The term *soliton* requires some explanation when applied to the three-wave interaction. The original definition of soliton has gradually altered in optics, and at the present moment most researchers define a soliton as a wave which propagates preserving its shape because of a balance between nonlinearity and dispersion for temporal solitons (between nonlinearity and diffraction for spatial solitons). Such waves were initially called solitary waves, and the term soliton reserved for solitary waves with a remarkable interaction property [20]: *A soliton is a solitary wave which asymptotically preserves its shape and velocity upon nonlinear interaction with other solitary waves, or more generally, with another (arbitrary) localized disturbance*.

The IST analysis in Refs. [12,13] shows that in the FSF case ($v_1>v_3>v_2$) both fundamental frequency waves have solitons with sech profiles and specific height to width ratios with this interaction property. These waves with the sech profiles are the fundamental solitons in the TWI theory. In Ref. [11], the soliton profiles for the TWI system (1) are

$$A_j(t,z)=A_{j,0}\,\mathrm{sech}\left[\frac{A_{j,0}}{\gamma_j}\left(t-\frac{z}{v_j}+\delta\right)\right], \tag{2}$$

where z is the propagation coordinate, t is time, and δ is an arbitrary time shift; $j=1$ gives the first fundamental wave, and $j=2$ the second, $A_{1,0}$ and $A_{2,0}$ are the initial amplitudes of the first and second fundamental pulses, respectively, and the coefficients γ_j which prescribe the amplitude/duration relationships are

$$\gamma_1=\sqrt{\nu_{1,2}\nu_{1,3}},\quad \gamma_2=\sqrt{\nu_{1,2}\nu_{2,3}},$$
$$\gamma_3=\sqrt{\nu_{1,3}\nu_{2,3}},\quad \text{with}\quad \nu_{i,j}=\left|\frac{1}{v_i}-\frac{1}{v_j}\right|. \tag{3}$$

In Ref. [11] these waves were termed TWI solitons to avoid confusion with and distinguish them from ''normal'' NLS solitons.

For the TWI system, each TWI soliton corresponds to a zero in either of the two outer diagonal elements of a 3×3 scattering matrix. Since the diagonal elements of the scattering matrix are the same before and after the interaction *i*, the TWI solitons (2) possess the interaction property common to all solitons: they recover their shape after interacting with another (arbitrarily shaped) fundamental frequency wave. In fact, for a fundamental TWI soliton the only effect of an interaction is a delay and possibly a phase change. Some examples of this behavior were given in Ref. [16].

The ZM scattering problem which underlies the IST for the TWI equations [12–17] is unwieldy and specialized. The ZM scattering problem is an eigenvalue problem for a linear system of three ordinary differential equations, and has not been extensively studied. Fortunately, the scattering problem for the TWI system (1) simplifies greatly if the three interacting waves are initially well separated. In this case, the ZM scattering problem factors into three (one for each frequency) simpler ZS scattering problems. The ZS problem is an eigenvalue problem (described in the Appendixes) for a linear system of two ordinary differential equations and is the basis for the IST solution of many nonlinear differential equations. In particular, the ZS scattering problem underlies the soliton theory for the nonlinear Schrödinger equation. As a result of the intense interest in NLS soliton data transmission, the ZS scattering problem has been extensively studied.

In our treatment of parametric amplification we will assume that the signal wave is predelayed, and that the signal enters the crystal sufficiently far behind the pump that we

can use the simpler ZS analysis. Output from numerical simulations quantifying the effect of varying the predelay (and hence overlap) of the signal relative to the pump are contained in the Appendixes. The conclusion to be drawn from these numerics is that the signal output from the decay of an intense pump is essentially independent of the extent of the predelay of the small trigger pulse.

This approach reduces the nonlinear interaction within the medium to an algebraic transformation of the input ZS scattering data (one for each frequency) to output ZS scattering data (again one for each frequency). To complete the analysis we need to know how to compute the ZS scattering data of arbitrarily shaped input pulses and how to recreate the output pulses from their ZS scattering data: this material is in the Appendixes.

The IST analysis [17,20–23] of Eq. (1) shows that under rather general conditions (such as the amplitude never crossing zero, etc. [17]) any smooth intense pulse at the frequency ω_i, well separated from the other two pulses, is almost entirely composed of TWI solitons. In fact, the normalized area of the pulse determines the number of solitons in the envelope

$$\mathcal{T}_i=\frac{1}{\gamma_i}\int_{-\infty}^{\infty}A_i(t)dt=\pi n_i+\epsilon_i \quad \text{with} \quad |\epsilon_i|<\frac{\pi}{2} \tag{4}$$

where $A_i(t)$ is the amplitude of the ith wave, the coefficients γ_i are given by Eq. (3), n_i is the number of TWI solitons contained in the ith wave, and ϵ_i is the nonsoliton or radiation portion of the ith wave. Equation (4) implies that pulses with $\mathcal{T}_i>\pi/2$ must contain TWI solitons, and that intense pulses ($\mathcal{T}_i\gg\pi$) are almost entirely composed of TWI solitons.

Each TWI soliton is described by two numbers: η (which we term the soliton amplitude) and D (which we term the nonlinear phase). All three waves may have multiple TWI solitons: when necessary we use two subscripts $\eta_{i,j}$ and $D_{i,j}$ on soliton parameters. The first index indicates the wave to which the soliton belongs: $i=1$ is the signal, $i=2$ is the idler, and $i=3$ is the high-frequency pump. The second index identifies the soliton within the wave. For example, $\eta_{2,4}$ is the amplitude of the fourth soliton in the idler envelope. Where it will not cause confusion (and the argument applies to all the envelopes), we drop the subscript identifying the wave to which the soliton belongs.

The three-wave interaction is nonlinear, and a pulse composed of n TWI solitons is not obtained by merely summing the single solitons [Eq. (2)]. When the pulses are separated the pulse profile is reconstructed using the ZS n-soliton formula [17]

$$Q(t)=2\sum_{j,k=1}^{n}D_j\exp[-(\eta_j+\eta_k)t](I+N^2)^{-1}_{j,k}, \tag{5}$$

where n is the number of solitons in the pulse; the soliton amplitudes are $\eta_1,\eta_2,\ldots,\eta_n$, which we will collectively refer to as the nonlinear spectrum; the nonlinear phases are $D_1,D_2,\ldots,D_n$; I is the identity matrix; the negative power denotes the matrix inverse; and the matrix N is

$$N_{k,j}=\frac{D_j\exp[-(\eta_k+\eta_j)t]}{\eta_k+\eta_j}. \tag{6}$$

The terminology spectrum and phases are deliberately chosen to highlight the analogy between the IST and the linear Fourier transform described below. Expressions (5) and (6) show that the multisoliton profiles have a scaling behavior similar to single solitons (2): if $Q(t)$ is an n-soliton profile with soliton amplitudes $\eta_1,\eta_2,\ldots,\eta_n$ and phases $D_1,D_2,\ldots,D_n$ then the scaled pulse $\beta Q(t/\beta)$ is an n-soliton pulse with soliton amplitudes $\beta\eta_1,\beta\eta_2,\ldots,\beta\eta_n$ and nonlinear phases $\beta D_1,\beta D_2,\ldots,\beta D_n$.

Since the ZS scattering problem describes the solitons in all three envelopes, the nonlinear superposition formula is similar for all three waves. Substituting the soliton spectrum $\eta_{i,1},\eta_{i,2},\ldots,\eta_{i,n}$ and nonlinear phases $D_{i,1},D_{i,2},\ldots,D_{i,n}$ for the ith pulse into Eq. (5) to obtain $Q_i(t)$ and scaling gives the amplitude for the ith pulse:

$$A_i(t)=\gamma_i Q_i(t). \tag{7}$$

Each wave will, in general, have a different number of solitons with different soliton amplitudes and nonlinear phases. The signal ($i=1$) pulse is $\gamma_1 Q(t)$, where $Q(t)$ is determined by Eq. (5) using the soliton amplitudes and nonlinear phases of the signal pulse. The number, amplitudes, and nonlinear phases of the solitons in the idler ($i=2$) pulse will not, in general, be the same as those in the signal pulse: the shape of the idler ($i=2$) pulse is $\gamma_2 Q_2(t)$, where $Q_2(t)$ is determined by Eq. (5) using the solitons in the *idler* pulse.

The nonlinear phases $D_1,D_2,\ldots,D_n$ appearing in expressions (5) and (6) for $Q(t)$ have a simple physical meaning: they determine the positions of the n TWI solitons in the pulse. In the simple case with only a single soliton in the ith pulse with amplitude $\eta_{i,1}$ and nonlinear phase $D_{i,1}$, Eqs. (5) and (6) give

$$A_{i,1}(t)=\mathrm{sgn}(D_{i,1})\,\gamma_i 2\,\eta_{1,i}\,\mathrm{sech}[2\,\eta_{i,1}(t-\tau_{i,1})]$$

$$\text{with} \quad \tau_{i,1}=\frac{\ln(|D_{i,1}|/2\eta_{i,1})}{2\,\eta_{i,1}}, \tag{8}$$

and the quantity $\tau_{i,1}$ gives the location of the peak of the single soliton. For a single TWI soliton the soliton coordinate τ is a natural parameter since it gives the location of the peak. However, τ does not determine the sign of the pulse and the nonlinear phase D which provides a complete description is the natural quantity to compute in the scattering problem. [Note that the peak amplitude of a single TWI soliton (8) in the ith envelope is $2\gamma_i\eta$, where η is the ''amplitude'' of the TWI soliton.]

We write

$$\tau_k=\frac{\ln(|D_k|/2\eta_k)}{2\,\eta_k}. \tag{9}$$

For a single soliton, or when solitons are far apart from each other, τ_k approximates the position of the center of the corresponding soliton. However, this simple interpretation of the phases is only valid when the solitons are well separated. The solitons interact strongly when they are nearby, and it

does not make sense to assign positions to individual solitons within a group. However, the notion of the soliton coordinates $\tau_1, \tau_2, \ldots, \tau_n$ defined by Eq. (9) is very useful. In fact, shifting all the soliton positions by the same amount τ_0 shifts the entire pulse by τ_0: in terms of the nonlinear phases $D_1, D_2, \ldots, D_n$ this means that Eq. (9), multiplying each of the soliton phases D_k in a pulse by $\exp[2\eta_k \tau_0]$, produces an identical pulse time shifted by τ_0.

The superposition of n solitons (or an nth-order soliton) is symmetric [24] if

$$D_k = \pm 2\,\eta_k \prod_{\substack{j=1 \\ j\neq k}}^{n} \frac{\eta_k + \eta_j}{\eta_k - \eta_j}. \tag{10}$$

Multisoliton superpositions can exhibit a wide range of complicated wave forms. The most important in practical applications are bell-shaped sech pulses. The combination [22] of n solitons with amplitude ratios $1:3:5:\ldots 2n+1$, i.e.,

$$\eta_j = \frac{2(n-j)+1}{2n-1}\,\eta_1 \quad \text{for } 1 \leqslant j \leqslant n, \tag{11}$$

and the phases given by Eq. (10), with all positive signs, has a sech shape with amplitude

$$\eta_1 - \eta_2 + \eta_3 - \cdots = \eta_1 \frac{2n}{2n-1}. \tag{12}$$

Selecting the largest soliton to have amplitude $\eta_1 = (n - 1/2)$ and $\eta_1 = 1 - 1/(2n)$ gives the useful amplitude distributions

$$\begin{aligned} Q(t) &= n\,\mathrm{sech}[(t-\tau)], \\ Q(t) &= \mathrm{sech}[1/n(t-\tau)]. \end{aligned} \tag{13}$$

For $n=1$, Eq. (13) is a fundamental soliton (first-order soliton) with the soliton amplitude $\eta_1 = \frac{1}{2}$. For integers $n>1$, Eq. (13) describes the decomposition of sech pulses (either n times longer or n times more intense than the fundamental soliton) into their constituent solitons. If n is not an integer, then profiles of form (13) are not pure n-soliton profiles but contain either m or $m+1$ (where m is the largest integer less than n) TWI solitons and some radiation.

Merely changing the signs of the soliton phasing in the input pulse gives a 25-fold intensity compression for a fifth-order soliton sech pulse. The intensity compression (obtained by changing all positive phases to alternating phases) for the nth-order soliton sech pulse is n^2. However, the secondary extrema in the compressed pulses can contain a significant portion of the pulse energy: in Fig. 1 the central peak of curve *a* contains ≈80% of the total pulse energy, while the secondary and tertiary peaks bear ≈13% and 6%, respectively, of the energy of the central peak. The duration of the central peak of curve *a* in Fig. 1 is $\approx \frac{1}{20}$th that of the sech pulse (curve *b*).

Another approach to soliton compression in the TWI is suggested by curve *c* in Fig. 1. This curve is the profile of the largest soliton contained in the fifth-order soliton pulse (curve *b*): the amplitude is 1.8 times that of curve *b*; the duration is $\frac{1}{9}$ times that of curve *b*, and it contains exactly 36% of the energy of curve *b*. Physically, within a long sech pulse there is always a soliton that has almost twice the amplitude of (and is substantially shorter) than the long sech pulse. In this example, if the largest soliton in the long sech pulse can be separated from the other solitons, then we achieve a compression ratio of 9 and a clean intensity distribution, and retain 36% of the energy in the compressed pulse.

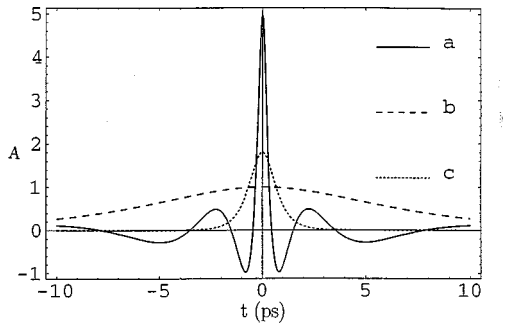

FIG. 1. Possible compression for a five-TWI-soliton sech profile: curve *a* is the amplitude *A* of an alternating phase symmetric five-soliton profile; *b* is the amplitude *A* of a sech profile with the same soliton content as *a*; and *c* is the amplitude *A* of the largest soliton in *b*.

The synchronously pumped optical parametric oscillator experiments [6,7] report a compression ratio of 20. Repeating the computation above shows that for a compression ratio of 20 the central soliton contains 20% of the initial energy. We believe that this is the type of compression observed in Refs. [6,7].

III. SOLITON SOLUTIONS: SOLITONS IN THE THIRD ENVELOPE AND NONLINEAR FOURIER TRANSFORM

In many ways, solving a nonlinear equation using an IST is analogous to solving the wave equation using the Fourier transform [20–23]. To solve a linear differential equation using the Fourier transform, one first decomposes an arbitrary initial wave into a superposition of simple plane waves. These plane waves do not change during the propagation, and so the spectrum is constant: only the phases of the plane waves change during the propagation. To complete the solution to the propagation problem, one computes the new phases from a simple evolution equation, and assembles the solution from the plane waves with their new phases.

Analogous to the linear Fourier transform, in the nonlinear case each of the three nonoverlapping input pulses [$A_{i,0}(t)$, where $i=1$, 2, and 3, respectively, are the initial signal, the idler, and the high-frequency pump] can be represented as a *nonlinear* superposition of n_i solitons with different amplitudes $\eta_{i,k}$ for $1 \leqslant k \leqslant n_i$ (which, to emphasize the analogy with the linear Fourier transform, we refer to as the ''soliton spectrum'') with associated nonlinear phases $D_{i,k}$ and some residual radiation. As in the linear case, the solitons (in the linear case spectrum) do not change during the interaction; however, their phases do. To find the shapes of the waves after the nonlinear interaction, one needs to construct the final envelopes, using the same solitons, but with

the new phases which the solitons have acquired during the nonlinear interaction.

Suppose that initially there is only an intense pump and a small signal wave with the highest speed v_1, i.e., the idler wave with speed v_2 is absent before the interaction. This is similar to parametric amplification when at the start of the interaction a small trigger pulse (signal wave) at frequency ω_1 is behind an intense pump pulse at frequency $\omega_3=\omega_1+\omega_2$, and during the interaction the signal overtakes the pump. Any time the high-frequency pump contains a soliton, it is unstable. When each pump soliton decays, it emits exactly one soliton into each daughter wave. Thus each soliton in the pump can be thought of as a bound state of zero binding energy, consisting of a signal and an idler soliton with perfectly matched energies: the matching is exactly that prescribed by the Manley-Rowe relations. The interaction of an intense pump with a small trigger pulse breaks the perfect energy balance and initiates the decoupling into idler and signal waves [12,13]. During the interaction, all solitons in the pump split and move to the idler and signal waves [12,13]: the number of solitons in each fundamental equals the number of solitons initially in the pump. However, the phases of each soliton will be changed by the interaction. We obtain analytical expressions for the final phases using an approach developed in Ref. [17].

When a soliton $\eta_{3,k}$ in the third envelope splits, it produces two low-frequency solitons: one with amplitude $\eta_{1,k}$ in the first envelope and one with amplitude $\eta_{2,k}$ in the second envelope with

$$\eta_{1,k}=\alpha_1\eta_{3,k} \quad \text{and} \quad \eta_{2,k}=\alpha_2\eta_{3,k}, \tag{14}$$

where the scalings α_1 and α_2 are

$$\alpha_1=\frac{\nu_{3,2}}{\nu_{2,1}} \quad \text{and} \quad \alpha_2=\frac{\nu_{3,1}}{\nu_{2,1}}. \tag{15}$$

If the n pump solitons are $\eta_{3,k}$ for $1\leqslant k\leqslant n$, then the signal and idler solitons are $\eta_{1,k}=\alpha_1\eta_{3,k}$ and $\eta_{2,k}=\alpha_2\eta_{3,k}$, respectively, for $1\leqslant k\leqslant n$. The nonlinear phases of the output solitons can be computed from an algebraic expressions for the output scattering matrix. Once the nonlinear phases are known the dominant soliton portion of the output is readily computed from the nonlinear superposition [Eqs. (5) and (6)].

As Eq. (4) shows, an intense pulse with $\mathcal{T}_i\gg\pi/2$ is essentially composed of TWI solitons since $\epsilon_i\ll\mathcal{T}_i$. We neglect the radiation (nonsoliton) part of the pump, and assume that the pump consists entirely of TWI solitons. Figure 2 shows representative output from the decay of a 4 sech(t) pump with a small trigger pulse: for case 1 the trigger is $0.05\exp(-t^2)$, while for case 2 the trigger is $0.0025\exp(-t^2)$. The features to note are that the four solitons [Eq. (13)] contained in the 4 sech(t) pulse have split according to Eq. (14), and are clearly visible in both the signal and idler output; the phases in the signal output alternate; the phases in the idler output do not alternate; the most intense soliton is in the lead in both pulses; and smaller trigger pulses increase the separation of the output solitons. The IST theory gives a very clear explanation of this behavior. In Ref. [25] we gave an analytical formula describing the behavior of the signal

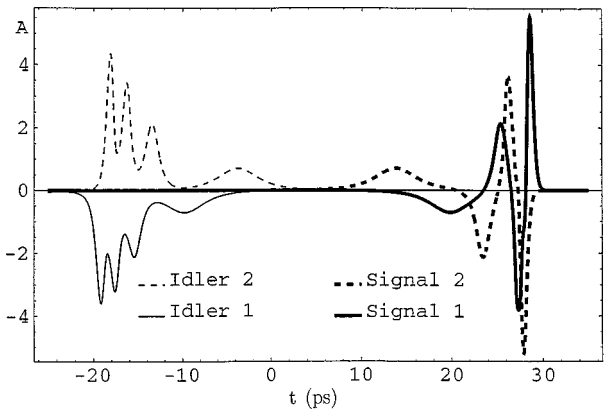

FIG. 2. Signal and idler amplitudes (A_1 and A_2) output from the decay of a four-TWI-soliton [4 sech(t)] pulse: signal and idler 1 are the output with trigger $0.0025\exp(-t^2)$; signal and idler 2 (multiplied by -1 to make the figure clearer) are the output with trigger $0.05\exp(-t^2)$.

wave. Here we complete the investigation by including the expressions for the idler. The derivation of the analytical expressions is in the Appendixes.

The following expressions for the final phases of the first (signal) and second (idler) solitons in terms of the initial parameters explain the behavior in Fig. 2:

$$D_{1,k}^{(f)}=\rho_1(\eta_{3,k})2\alpha_1\eta_{3,k}\prod_{\substack{j=1\\ j\neq k}}^{n}\frac{\eta_{3,k}+\eta_{3,j}}{\eta_{3,k}-\eta_{3,j}}\exp\left[\frac{2\eta_{1,k}}{v_1}z\right], \tag{16}$$

$$D_{2,k}^{(f)}=\rho_1(\eta_{3,k})\alpha_2 D_{3,k}^{(i)}\exp\left[\frac{2\eta_{2,k}}{v_2}z\right], \tag{17}$$

where $D_{3,k}^{(i)}$ are initial phases in the pump, $D_{1,k}^{(f)}$ and $D_{2,k}^{(f)}$ are final soliton phases in the signal and the idler waves, and $\eta_{3,1},\eta_{3,2},...,\eta_{3,k}$ are the initial pump solitons; the parameters α_1 and α_2 are defined in Eq. (15), and ρ_1 is the ZS reflection coefficient of the first (signal) wave. As shown in the Appendixes, if the initial signal pulse $A_{1,0}(t)$ is small, then

$$\rho_1(\eta)\simeq\frac{1}{\gamma_1}\int_{-\infty}^{\infty}A_{1,0}(t)\exp(-2\alpha_1\eta t)dt. \tag{18}$$

When using Eq. (16), one should bear in mind that due to the way this expression was obtained (see the Appendixes), the phases $D_{1,k}^{(f)}$ define the final shape of the time reversal of the signal pulse.

Expressions (16) and (17) show a dramatic difference in the behavior of the signal and idler waves. The final signal phases $D_{1,k}^{(f)}$ depend only on the initial soliton content of the pump, and *do not* depend on the initial nonlinear phases of the pump solitons. This is very surprising: in general one would expect the output shape of the signal wave to involve both soliton amplitudes $\eta_{3,k}$ and nonlinear phases $D_{3,k}^{(i)}$. A linear analogy to this would be if the propagation of a beam did not depend on the initial shape of its wave front. For the nonlinear case, the fact that Eq. (16) does not involve the initial nonlinear phases $D_{3,k}^{(i)}$ but only the soliton amplitudes

$\eta_{3,k}$ means that the output shape of the signal wave practically does not depend on the initial shape of the pump.

In contrast, the initial phases $D_{3,k}^{(i)}$ do appear in expression (17) for the final $D_{2,k}^{(f)}$ idler soliton phases, and the idler output depends on the initial profiles of the intense pump (through the initial soliton phases) as well as the reflection coefficient $\rho(\eta_{3,k})$ (or radiation spectrum at the points $\eta_{3,k}$) of the small trigger.

The final shape of the signal depends critically on the product

$$\Psi_k = \prod_{\substack{j=1 \\ j\neq k}}^{n} \frac{\eta_{3,k}+\eta_{3,j}}{\eta_{3,k}-\eta_{3,j}}, \tag{19}$$

which determines the signs of the solitons in Eq. (16). There is no loss of generality in assuming the solitons are ordered, i.e., $\eta_{3,k} \geqslant \eta_{3,k+1}$, which ensures $\Psi_1>0$, $\Psi_2<0$, $\Psi_3>0$, etc. It is these alternating signs that give the output signal pulse the characteristic profile of a decaying parade of oscillating humps, which can be seen in Fig. 2. In contrast, the output idler soliton phases [Eq. (16)] are determined by the initial pump soliton phases $D_{3,k}$. If the soliton phases in the pump are initially positive (which is the case for the sech pump pulse in Fig. 2), then the output idler phase will also be positive (as is shown in Fig. 2).

The exponential factors in Eqs. (16) and (17) have no influence on the output pulse shapes. As discussed above, these exponential factors correspond to uniform translations of the output pulses. In fact, they show that the solitons in Eqs. (16) and (17) move with velocities v_1 and v_2, respectively. Calculating the soliton coordinates (9)—dividing Eq. (16) by twice the soliton amplitude, taking logarithms, and dividing again—gives the soliton ''coordinates'' of the output signal and idler solitons ($\tau_{1,k}^{(f)}$ and $\tau_{2,k}^{(f)}$, respectively)

$$\tau_{1,k}^{(f)} = \frac{z}{v_1} + \frac{\ln \rho_1(\eta_{3,k})}{2\eta_{1,k}} + \frac{\ln(\Psi_k)}{2\eta_{1,k}}, \tag{20}$$

$$\tau_{2,k}^{(f)} = \frac{z}{v_2} + \frac{\ln \rho_1(\eta_{3,k})}{2\eta_{2,k}} + \frac{\tau_{3,k}^{(i)}}{\alpha_2}. \tag{21}$$

The first terms in Eqs. (20) and (21) arise from the exponential factors in Eqs. (16) and (17), and show that all the output TWI solitons move with the same speed (v_1 for the signal, and v_2 for the idler). The second term shows how the trigger pulse profile $A_{1,0}$ effects each soliton in the pump through the reflection coefficient ρ_1. When the reflection coefficient is small, the solitons in the signal wave experience large time delays and the solitons in the idler are advanced. Small solitons, corresponding to small η_k, experience larger time shifts and will be delayed or advanced more by the nonlinear interaction: therefore, the generic output signal wave is an ordered train of TWI solitons, as illustrated in Fig. 2. Smaller initial amplitudes of the signal wave produce bigger time shifts. Figure 2 shows the output for two different input signal intensities: in agreement with theory, the smaller signal input produces longer delays and increased separation of the output solitons. [Note that Eqs. (16) and (20) give the phases and coordinates of the time-reversed signal output.] The third terms, determined entirely by the pump, show the effect of the other TWI solitons in the pulse: for the signal wave this term is independent of the coordinates $\tau_{3,k}^{(i)}$ of the input pump pulse. For the idler this term is a scaled copy of the coordinates $\tau_{3,k}^{(i)}$. For small trigger pulses, the terms involving $\rho(\eta_{3,k})$ are dominant in Eqs. (20) and (21) and the third terms are negligible. This shows that for small triggers the time shift increases as the soliton amplitude decreases which explains the ordering of the solitons in Fig. 2.

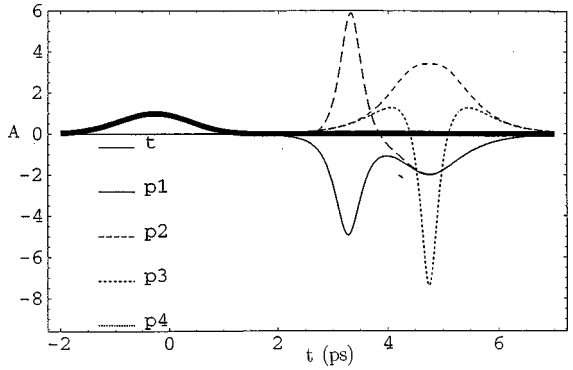

FIG. 3. Initial amplitudes for numerical verification. The pulse (t) is the fundamental trigger pulse while $p1-p4$ are pump profiles. All four pump pulses have the same soliton amplitudes ($\eta_1=2.7$ and $\eta_2=1$); they differ in their soliton phases.

Numerics on system (1), illustrating the analytical predictions, are contained in Figs. 3 and 4. Figure 3 shows a single trigger pulse with four different pump pulses: all four pump pulses are pure two-soliton profiles with $\eta_1=2.7$ and $\eta_2=1$, but with different soliton phases. Equations (16) and (17) predict that the signal output of this trigger pulse with these three different pump profiles should be identical. Figure 4 shows the numerical signal and idler output: the signal output is the same for the four different pumps, while the idler essentially repeats the pump profile. In practice, of course, pulses will never have exact soliton profiles, and there will always be small amounts of radiation. Additional numerics illustrating the stability of the soliton behavior are in Ref. [25].

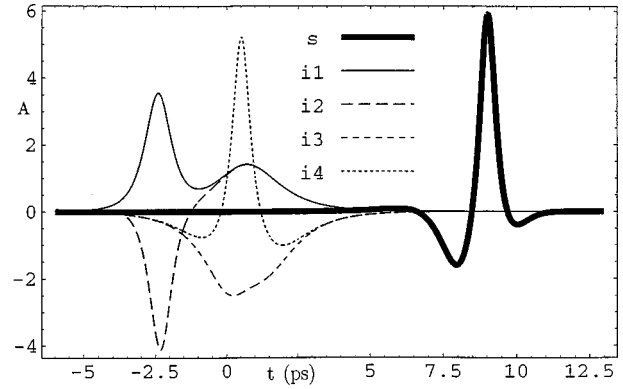

FIG. 4. Signal and idler output amplitude from numerical verification. The pulse (s) is the common signal output predicted analytically (the outputs from all four processes are indistinguishable). The pulses $i1-i4$ are the idler outputs that for the particular choice of trigger with $\overline{\rho}(2.7)=\tilde{\rho}(1.0)=1$ should reproduce the input pump profiles $p1-p4$ in Fig. 3: the slight deviations are due to the use of the approximate expression for ρ.

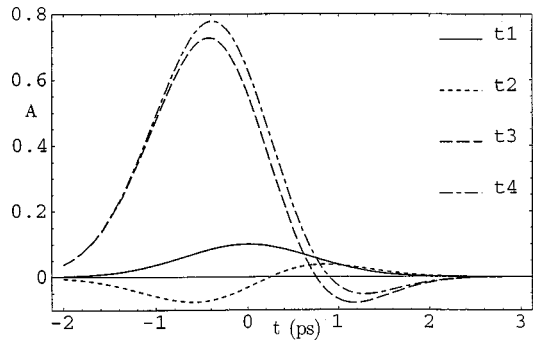

FIG. 5. Trigger signal amplitude input for a numerical demonstration of the control of soliton positions. The pump for all four trigger pulses is a two-soliton 2 sech(t) profile.

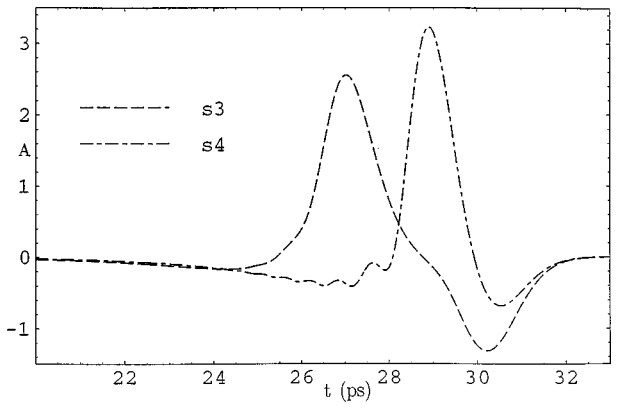

FIG. 7. Signal amplitude output from triggers 3 and 4 in Fig. 5.

Expressions (16)–(21) show that the shape of the trigger pulse controls the position of the output solitons in the signal and idler waves. In Ref. [25] we showed that for small Gaussian triggers the solitons emerge ordered by amplitude in increasing order. In this paper we extend this analysis to show how to adjust the positions of the output solitons by changing the shape of the input trigger pulse.

If the parameter $\rho_{3,k}$ in Eqs. (20) and (21) is near zero, then the kth soliton in the signal or idler waves experiences an extreme time shift during the interaction. Since the parameter $\rho_{3,k}$ is determined by the initial signal profile, one can control the positions of the output solitons by altering the shape of the signal trigger. It is possible to isolate the largest soliton by selecting triggers which delay the other smaller solitons. If $\rho(\eta_{3,k})=1$ [or, more generally, $\rho=\exp(q\eta_{1,k})$ for some q] for *all* pump TWI solitons, then the output signal phases [Eq. (16)] satisfy Eq. (10), with alternating phases, while the output idler phases are a scaled copy of the input phases: in this case the signal output is the symmetric profile with alternating soliton phases and the idler output repeats the pump profile. The alternating phases superposition provides the maximum intensity and compression of the pulse. However, these profiles have satellite peaks containing a substantial fraction of the energy. Note that the idler output repeats the pump profile when the signal output is the maximal amplitude symmetric profile. Figures 5–7 show some of the possibilities for controlling the shape of the output pulses. Figure 5 shows four different trigger profiles: $(t1)$ is $0.2\exp(-t^2)$, which is included to show the typical effect of a moderate trigger; $(t2)$ is $(0.450t-0.112t)\exp(-t^2)$, which is designed to delay the emission of the small soliton; $(t3)$ is $(0.556t-0.742t)\exp(-t^2)$, which is designed to delay the emission of the large soliton; and $(t4)$ is $(0.631t-0.706t)\exp(-t^2)$, which is designed to produce symmetric peak compression output for the idler and simultaneously reproduce the signal profile.

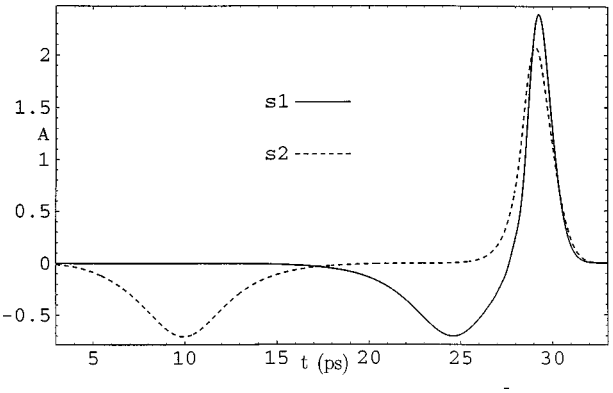

FIG. 6. Signal amplitude output from triggers 1 and 2 in Fig. 5.

Figures 6 and 7 show the signal output from the decay of the 2 sech(t) pulse (a symmetric two-soliton profile [Eq. (13)] containing solitons with amplitudes $\frac{3}{2}$ and $\frac{1}{2}$) with the four triggers in Fig. 5. The idler outputs are pure two-soliton pulses. The signal radiation (from the trigger) is visible at the rear of the fourth pulse in the signal output. The Gaussian pulse $(t1)$ produces a generic output with the two solitons fairly close together. Trigger $(t2)$ which was chosen to make $\rho(0.5)\simeq 0$ by setting approximation (18) equal to zero, produces, as predicted by Eq. (20), a substantial delay of the small $\eta_2=0.5$ soliton and results in substantial separation between the output solitons. Trigger $(t3)$ which was chosen to make $\rho(1.5)\simeq 0$ by setting approximation (18) equal to zero, delays, as predicted by Eq. (20), the large $\eta_{3,1}=1.5$ soliton. Trigger $(t4)$, which was chosen to make $\rho(0.5)\simeq\exp(-0.5)$ and $\rho(1.5)\simeq\exp(-1.5)$, produces, as predicted by Eqs. (16) and (17), symmetric output for both the signal and idler, with the idler repeating the pump profile and the signal showing maximal compression with alternating phases between the solitons.

Delaying the second soliton (Fig. 6, curve 2) generates a single, clean-profile, compressed soliton pulse from a multisoliton pulse. If the process is stopped after only the largest soliton is formed, the output pulse will have a clean sech profile with the duration (much less than the pump duration for an intense pump) of the largest pump soliton. For the two-soliton 2 sech(t) pulse, the output signal duration is $\sqrt{2}/3$ that of the pump. The effect is more dramatic for pumps containing more solitons: for the n-soliton n sech(t) pulse, the duration of the pulse obtained by isolating the largest soliton [Eq. (13)] is $\sqrt{2}/(2n-1)$ times that of the pump. In this case the fraction of the pump energy contained in the smaller TWI solitons is lost. For stronger compressions more energy is lost. Nevertheless, the energy of the largest pump TWI soliton is considerable. For example, 20-fold compression is possible with an energy conversion of 20%. This matter is discussed in detail in Sec. IV.

Another compression possibility is to generate symmetric distribution (10) by making the reflection coefficient $\rho(\eta_{3,k})$

equal to 1 simultaneously for all the pump solitons to produce the peak soliton interaction (Figs. 5 and 7, curves 4). This generates stronger compression at the cost of satellite pulses. For the two-soliton 2 sech(t) pulse in Fig. 7 ($s4$), the output signal amplitude is about three times greater than that of the pump. The effect is more dramatic for pumps containing more solitons: for the n-soliton n sech(t) pulse, the amplitude compression by creating the optimal alternating phases [Eq. (10)] is close to n times with a very short duration. Although energy conversion is high in this second type of compression, the appearance of satellite pulses is a major drawback.

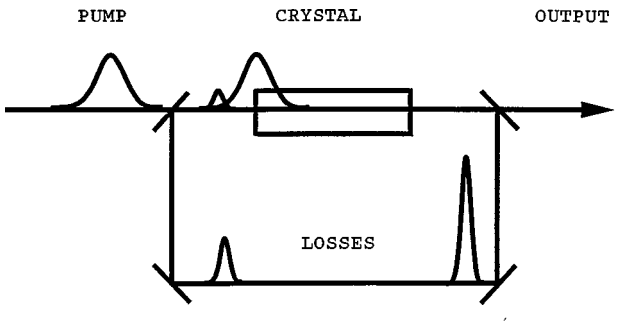

FIG. 8. Schematic of experiment.

IV. EXPERIMENTAL OBSERVATION OF TWI-SOLITON BEHAVIOR

In this section we compare predictions of the TWI-soliton theory with the experimental results observed in Refs. [6,7] for an experimental synchronously pumped optical parametric oscillator (SPOPO). Dispersion is extremely small in this SPOPO, and the observed soliton behavior cannot be attributed to the well-known cascaded quadratic nonlinearity ($\chi^{(2)}\times\chi^{(2)}$) soliton like waves which can appear only in strongly dispersive quadratic media.

There is difference between the notation of the present paper and Refs. [6,7]. The present paper considers parametric amplification which corresponds to the steady-state regime in the SPOPO. In the theoretical section of this paper the ''signal'' refers to the trigger wave initially present before the interaction. In Refs. [6,7], the signal wave refers to the highest frequency (and intermediate speed) fundamental wave. To avoid confusion we will continue to refer to the fastest fundamental wave as the signal.

The experimental SPOPO [6,7] consists of a transverse walk-off compensated two-barium-borate (BBO) crystal configuration pumped by the third harmonic (355 nm) of a pulsed Nd:YAG (yttrium aluminum garnet) laser. The third harmonic pump consist of approximately 60×11-ps pulses with the energy of a single pulse up to 50 μJ. The 0.7-mm pump-beam diameter within the crystals gives virtually totally overlapped propagation of the pump and oscillating radiation along both crystals. The SPOPO oscillates at frequencies from 400 to 2300 nm. The balance of each round trip between losses at the optical elements and the nonlinear interaction with a fresh pump pulse determine the output of the SPOPO. The time delay between the oscillating pulse and individual pump pulses at the input of the first crystal is determined by the SPOPO cavity round-trip time. This time delay is controlled by cavity length detuning (ΔL) from the length at which the energy threshold for oscillation is a minimum. When $\Delta L>0$ the SPOPO cavity round-trip time is greater than the interval between pump pulses, and the oscillating pulse enters the crystal behind the pump every round trip. A schematic of the experimental setup is shown in Fig. 8. The main results of the experiment are the following.

(i) Compression (up to 20-fold) is due to the pronounced *group-velocity mismatch* of the pump and oscillating wave in the nonlinear crystal. The compressed pulses exhibit *soliton-like* behavior: the signal (fastest) rapidly reaches a steady state with stable pulses. Second-order dispersion effects (GVD) did not have substantial influence on process.

(ii) Compression takes place only when the SPOPO is well above threshold. The duration of the compressed wave decreases as the *pump intensity increases*.

(iii) Only the *faster* of the signal and idler pulses can be compressed. (In Refs. [6,7], the fastest wave was referred to as the ''idler''; in this paper the fastest wave is the ''signal.'')

(iv) At a high pump level, a number of pulses are generated in the signal envelope.

As shown below, these observed phenomena are surprisingly well matched with the TWI-soliton theory of OPG processes. The general three-wave interaction theory [12–17] identifies two distinct regimes depending on whether the group velocity of the high frequency pump does or does not lie between the speeds of the idler and signal. The regimes are FSF, when the high-frequency group velocity is between the velocities of the signal and idler; and SFF, when the pump group velocity is *not* between the velocities of the signal and idler.

The behavior of the intermediate wave in the SFF regime for parametric generation is very interesting. Extensive numerical calculations show that it generally (except for extreme cases when the speeds of the interacting waves are very close to each other) emerges as a single hump with a very clean profile. We cannot explain this behavior analytically now: this case requires further development of the IST theory. Extending the theory to this case would be very interesting for two reasons. The first reason is that in normally dispersive nonlinear media the intermediate speed wave is the higher frequency output pulse, and compression of this envelope would give a high-frequency tunable radiation source. The second reason is the very clean temporal profile of the intermediate speed pulse particularly the absence of a tail.

The experiment [6,7] is in the SFF regime, since the experimental conditions ($\lambda_3=0.53\,\mu$m, $\lambda_2=0.48\,\mu$m, and $\lambda_3=1.3\,\mu$m) in BBO give—all optical data is from Ref. [26]—group velocities of $v_3=1.67\times10^{10}$ cm/sec, $v_2=1.7\times10^{10}$ cm/sec, and $v_1=1.78\times10^{10}$ cm/sec. In the SFF regime TWI-soliton theory predicts that only the fastest (signal) envelope can contain TWI solitons: so in the experiment TWI-soliton compression is only possible for the fastest wave. This theoretical prediction agrees very well with the experimental data, where no compression was observed for the intermediate speed wave. Such a clear indication of the distinction between the two waves predicted by theory, and observed in experiment is a strong argument for the soliton nature of the parametric compression. However, a rigorous

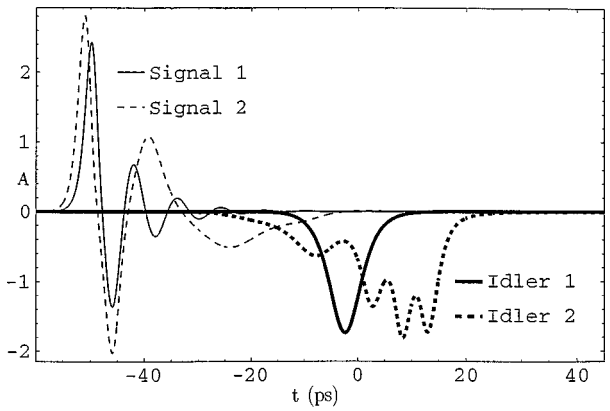

FIG. 9. Comparison of the signal and idler amplitude output from the decay of a 2 sech(t/4) pump in different velocity regimes. Signal and idler 1 are the SFF case. Signal and idler 2 are the FSF soliton decay case. In both cases the pump is 2 sech(t/4), the trigger is 0.05 sech(t), and the frame of reference is moving at the average of the extreme velocities. Note the marked qualitative similarity of the leftmost portion of the signal curves.

analysis of the experiment requires the complete analytic theory for the SFF regime: unfortunately this theory is not as advanced as FSF theory. We anticipate future theoretical advances will provide the analytical tools to complete an exact quantitative picture of the SFF process.

Here we attempt to explain the SFF process qualitatively using the well-developed FSF theory. Our qualitative description is based on the numerically observed fact that the behavior of the fastest wave (which can carry TWI solitons) in the SFF regime is surprisingly close to the behavior of the fastest wave in an associated FSF regime: the FSF regime ''corresponding'' to a SFF regime is obtained by interchanging the group velocities of the idler and the pump. Numerical calculations show that the output shape of the fastest (signal) wave are very close for these two cases. In fact, when the initial shape of the pump is Gaussian, the output shape of the fastest wave is always the sequence of decreasing-amplitude, oscillating humps predicted by the rigorous FSF theory. The area of the first hump (which is the largest soliton in the FSF case but is *not* a soliton in the SFF case) is within a few percent of π in the SFF case. However, the following pulses have areas considerably smaller than the ''soliton area'' of π. The height and duration of the leading pulse are also very close for the corresponding SFF and FSF cases. The behavior of the slower (idler) wave is completely different for the SFF and FSF cases.

Figure 9 compares numerical simulations of parametric amplification in the FSF and SFF regimes: signal 1 and idler 1 are from the experimental SFF parameters $v_3=1.67\times10^{10}$, $v_2=1.71\times10^{10}$, and $v_1=1.78\times10^{10}$; signal 2 and idler 2 are from the FSF parameters obtained by interchanging v_2 and v_3, i.e., $v_2=1.67\times10^{10}$, $v_3=1.71\times10^{10}$, and $v_1=1.78\times10^{10}$. Note that the signal pulses (particularly the most intense lefthand portions) are similar in both cases, and that idler 1 (as predicted by theory) does not have the distinguishing solitons characteristics of idler 2.

This analogy between the behavior of the fastest waves for the SFF and associated FSF regimes allows us to give a qualitative explanation of the behavior of the fastest wave in the SFF case by using the FSF theory. In the remainder of this section we describe the behavior of the fastest (signal) wave by considering the corresponding FSF regime, obtained by switching the idler and pump group velocities. Tables I and II summarize the soliton content of sech profile pump pulses for the corresponding FSF regime in which the pump wave contains solitons. In the FSF case these pump solitons split and emerge according to the theory developed earlier in this paper: the lead pulses in the SFF and FSF cases are qualitatively similar. The similarity between the two FSF

TABLE I. Soliton content of n sech(t) pump pulses (FSF regime). The first three columns contain the peak amplitude, width, full width at half maximum of intensity (FWHMI), and soliton content [Eq. (13)] of an n sech(t) pump pulse. The next two columns contain the peak amplitude and width (FWHMI) of the largest soliton in the pump; the adjacent columns contain the compression obtained by isolating the largest soliton and the percent of the pump energy it contains. The last column is the amplitude (twice the sum of the solitons) of the pulse formed from the same solitons with symmetric alternating phases [Eq. (10)].

	n sech(t) pump			Largest soliton				Alternating phases
n	Amp.	Width	η's	Amp.	Width	Comp.	Energy %	Amp.
1	1	1.762	$\frac{1}{2}$	1	1.762	1	100	1
2	2	1.762	$\frac{1}{2},\frac{3}{2}$	3	0.587	3	75	4
3	3	1.762	$\frac{1}{2},\frac{3}{2},\frac{5}{2}$	5	0.352	5	56	9
4	4	1.762	$\frac{1}{2},\frac{3}{2},\frac{5}{2},\frac{7}{2}$	7	0.652	7	44	16
5	5	1.762	$\frac{1}{2},\frac{3}{2},\frac{5}{2},\frac{7}{2},\frac{9}{2}$	9	0.696	9	36	25
n	n	1.762	$\frac{1}{2},\frac{3}{2},\ldots,n-\frac{1}{2}$	$2n-1$	$\frac{1.762}{(2n-1)}$	$2n-1$	$100\left(\frac{2}{n}-\frac{1}{n^2}\right)$	n^2

TABLE II. Soliton content of sech(t/n) pump pulses (FSF regime). The first three columns contain the peak amplitude, width (FWHMI), and soliton content [Eq. (13)] of an n sech(t) pump pulse. The next two columns contain the peak amplitude and width (FWHMI) of the largest soliton in the pump: the adjacent columns contain the compression obtained by isolating the largest soliton and the percent of the pump energy it contains. The last column is the amplitude (twice the sum of the solitons) of the pulse formed from the same solitons with symmetric alternating phases [Eq. (10)].

	sech(t/n) pump			Largest soliton				Alternating phases
n	Amp.	Width	η's	Amp.	Width	Comp.	Energy %	Amp.
1	1	1.762	$\frac{1}{2}$	1	1.762	1	100	1
2	1	3.524	$\frac{1}{4},\frac{3}{4}$	$\frac{3}{2}$	1.175	3	75	2
3	1	5.286	$\frac{1}{6},\frac{3}{6},\frac{5}{6}$	$\frac{5}{3}$	1.057	5	56	3
4	1	7.048	$\frac{1}{8},\frac{3}{8},\frac{5}{8},\frac{7}{8}$	7/4	1.007	7	44	4
5	1	8.810	$\frac{1}{10},\frac{3}{10},\frac{5}{10},\frac{7}{10},\frac{9}{10}$	9/5	0.979	9	36	5
n	1	1.762 n	$\frac{1}{2n},\frac{3}{2n},\ldots,1-\frac{1}{2n}$	$2-\frac{1}{n}$	$\frac{1.762n}{(2n-1)}$	$2n-1$	$100\left(\frac{2}{n}-\frac{1}{n^2}\right)$	n

and SFF fastest waves in Fig. 9 is due to *quasisoliton* behavior. Qualitatively, the analogy is explained by the area theorem (4), which ensures that any wave which can contain TWI solitons (such as the fastest wave in the SFF case) does contain solitons if it has normalized area exceeding $\pi/2$. In the SFF case the fastest wave had no solitons before the interaction (it was small), and since it can gain no solitons from the pump (in the SFF case the pump has no solitons) it must have no solitons after the interaction and must change phase to avoid violating the area theorem. Although the numerics show striking analogies between the behavior of the fastest waves in the SFF and FSF regimes, many features of the SFF regime are unknown. Future rigorous investigation, using IST theory, may reveal many unknown features of the SFF process. In fact, preliminary analytical consideration of the SFF regime shows that the pump will have TWI solitons if the signal and the pump waves significantly overlap at the start of the interaction. However, the rigorous theory for the SFF case is beyond the scope of this paper.

The FSF theory developed in this paper shows that parametric amplification of small signal pulses is extremely stable with respect to trigger pulse intensity. The TWI-soliton explanation of this stability is simple: the parametric process output is a train of TWI solitons determined by the number and size of the TWI solitons contained initially in the pump. Varying the trigger pulse intensity changes the time-delays between the emerging TWI solitons but does not change the general shape of the output signal and idler. Moreover, expressions (20) and (21) predict a slow logarithmic dependence of the time delay on trigger intensity. Even large variations of the trigger pulse intensity produce only small changes in the output: in Fig. 2, increasing the trigger intensity by a factor of 400 produces only minor changes in the output train of five TWI solitons. Combined with the stability of the process with respect to the pump shape, discussed in the previous sections, this feature makes TWI-soliton parametric amplification extremely stable. The FSF-SFF analogy suggests that the development of steady-state pulses and insensitivity to losses observed in the experiment were a SFF analogy of this FSF TWI-soliton stability. Incidentally, the parametric decay process does not possess this stability when when none of the waves can contain TWI solitons. In the nonsoliton quasistationary ($v_1=v_2=v_3$) regime, the process output is extremely sensitive to small variations in the trigger pulse.

There are two main soliton compression mechanisms for parametric amplification. Maximal compression is achieved if after the interaction the output TWI solitons have alternating sign ''symmetric'' [Eq. (10)] phases: the parametric decay produces such output [Eq. (16)] if the trigger pulse gives $\rho(\eta_k)=1$ for all the pump TWI solitons [or, more generally, $\rho(\eta_k)=\exp(q\eta_k)$ for an arbitrary real constant q]. Figure 5 ($t4$) shows a trigger that does this for a two soliton pulse: curve ($s4$) in Fig. 7 shows the maximally compressed signal output while the idler duplicating the pump profile. Tables I and II give compressions for sech profile pump pulses.

The second type of parametric amplification compression is to isolate the dominant pump soliton. As shown by Eqs. (16) and (17) or (20) and (21) for small triggers, the largest soliton is the first to emerge. Figures 2 and 9 show the output of the nonlinear process when the interaction length is very long. In practice, the nonlinear interaction is interrupted long before all the pump solitons emerge. For an intense pump pulse containing many TWI solitons the output signal pulse is a single, substantially compressed, clean TWI soliton if the length of the nonlinear medium is chosen so that only the first soliton forms. Longer or more intense pumps give higher compression. Tables I and II also give the compression values and the energy efficiency coefficients for sech profile pumps. These tables give the soliton parameters of

TABLE III. Parameters for comparison of theory and experiment.

	Phase matching angle (degrees)	Idler λ_1 μm	Idler v_1 cm/sec	Signal λ_2 μm	Signal v_2 cm/sec	Pump λ_3 μm	Pump v_3 cm/sec
Case 1	27	1.80	1.78×10^{10}	0.43	1.70×10^{10}	0.35	1.67×10^{10}
Case 2	30	1.30	1.79×10^{10}	0.47	1.72×10^{10}	0.35	1.68×10^{10}

the largest TWI soliton contained in pump. After this soliton moves to the signal wave its amplitude must be normalized according to relationships (14) and (15) and then (2) and (3). This normalization is important and in extreme cases can substantially alter the results. However, in the general case when the speeds of the three waves are well separated, Tables I and II give a good idea about the compression parameters.

A very attractive feature of compressing pulse by isolating the largest soliton is that the compression appears naturally: for small Gaussian trigger pulses Eqs. (16) and (17) show that the largest TWI soliton always emerges first. In practice, however, it is difficult to stop the interaction at exactly the right moment, and a second and even a third TWI soliton may also form: although this increases the process efficiency, it spoils the shape of the compressed pulse. To obtain cleaner output pulses, one should use less intense trigger pulses by introducing losses into the resonator: large losses in the resonator decrease the intensity of the trigger pulses and increase the separation of the output solitons producing cleaner output. This behavior was observed in the experiment. Another way to obtain clean pulses is to tailor the shape of the input signal pulse. Section III shows how to produce pulse profiles by designing the trigger to delay the appearance of the smaller TWI solitons. This technique can produce compressed pulses with very clean sech profiles. Curve $(t2)$ in Fig. 5 is the trigger giving the signal output $(s2)$ in Fig. 6: the smaller soliton is strongly delayed, and both the signal and idler output are clean.

Tables I and II show that the intensity of the largest soliton is approximately twice the pump intensity when there are more than three pump TWI solitons, and the duration of the largest soliton decreases rapidly as the pump energy increases. The primary drawback of compressing by isolating the largest soliton is that only the energy of the largest soliton is used (the pump energy in the smaller solitons is discarded), and the efficiency drops for high compressions. However, as the tables show, even for high compressions the largest soliton contains a significant portion of the initial pump energy. For example, ninefold compression can be achieved with an energy efficiency of 36%, and 20-fold compression with 20% efficiency. (Efficiency is defined as the fraction of the initial pump energy in the largest TWI soliton.) Note: 100% efficiency means that all the pump energy is transformed into the signal and idler. This energy is partitioned between the generated waves according to their frequencies and normalizations (2) and (3) and (14) and (15).

The experimental compression of the fastest wave observed in Refs. [6,7] was analogous in behavior to isolating of the largest TWI soliton. We compared the theory and the experiment at two different frequencies and phase matching angles. The parameters for the two cases are summarized in Table III. All the data are taken from Ref. [26], which gives the appropriate nonlinear coefficient for BBO as 2.3 pm/V. Estimating the pump energy shows that in the corresponding FSF case each pump pulse could contain 10–15 TWI solitons. Tables I and II predict that the largest pump soliton should be 20–30 times shorter than the pump. There are two factors that need to be accounted for: the first is the normalizations (14) and (15) describing the transfer of the pump TWI soliton to another envelope; the second is the amplification and compression which results from the proximity of TWI solitons in the train when the phases are alternating. For the experimental frequencies in BBO, these factors act in opposite directions, and approximately cancel. The theory predicts a compression of ~20 for a pump intensity of ~800 MW/cm^2, exactly what is observed in the experiment. The theory predicts higher compression for higher intensities; however, in the experiment the compression coefficient stabilized after the pump intensity reached 800 MW/cm^2. We believe this to be due to spatial pulse modulation, which is neglected in the theory.

In the experiments the nonlinear medium was roughly the length required for the first TWI soliton to form. For low intensity pumps [Fig. 10 (B)] the profile is clean without satellites because only the most intense TWI soliton has appeared: the compression is roughly a factor of 12. As the pump intensity increases the temporal output profile develops additional maxima [compare Fig. 10(A) with Figs. 2 or 9] because the nonlinear medium is now sufficiently long for the less intense solitons to form and spoil the clean profile. Theory predicts that the duration of the dominant pump soliton should be inversely proportional to the square root of the pump intensity. The 0.7-mJ pulse [Fig. 10(B)] has a duration of $\tau\approx850$ fs. Computing the proportionality constant using this value gives a prediction that the 1.8 mJ pulse [Fig. 10(A)] should have a duration of 530 fs, in good agreement

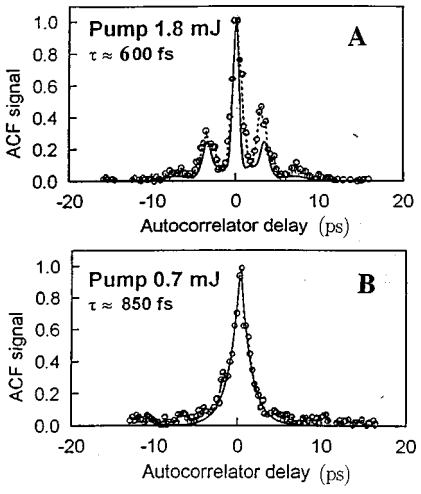

FIG. 10. Experimental results.

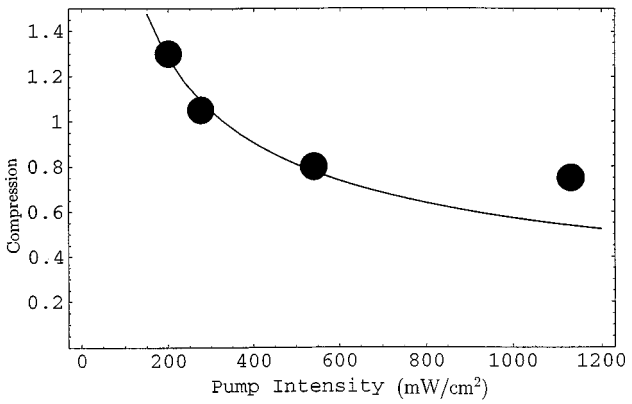

FIG. 11. Comparison of experiment and theory.

with the experimental value of ≈600 fs. Figure 11 compares the theoretical compression predictions with the experimentally measured values: for pump intensities <600 MW/cm^2 the theory provides a good fit with the experimental values. We believe the small discrepancy between theory and experiment for the last point on the graph is due to the spatial modulation of the waves.

V. CONCLUSIONS

The TWI-soliton theory gives a clear picture of some complicated features of parametric amplification. The ability to predict and control the form of the output pulses may have important practical applications in pulse compression, pulse shaping, and optical computing. Although the IST theory has existed since 1974, it is only recently that pulses sufficiently short and intense to test and use it have become technologically feasible. There is currently a growing body of experimental results that we believe can be described by this theory. In this paper we compared the experimentally observed 20-fold signal pulse compression in a synchronously pumped OPO with TWI theory. The experimental data is in a good agreement with TWI-soliton theory.

Although, the mathematical basis of TWI-soliton theory is already well developed, there are numerous questions which require more detailed investigation. In this paper, we considered the simplest FSF interaction in which all three interacting waves can have TWI solitons. For practical purposes it is very important to improve our understanding of the SFF interaction: because of normal dispersion the high-frequency pump is usually slower than the signal and idler. The SFF case is also very useful in the new periodically poled nonlinear media, because it allows the use of the large $d_{3,3}$ coefficient.

It is also important to develop the theory for initially overlapping pulses. This requires development of the Zakharov-Manakov scattering problem, which has thus far not attracted the attention of the research community. Further development of the ZM problem would allow us to consider overlapping initial pulse profiles: in practice the limited length of nonlinear media ensures that input pulses overlap. This overlap can considerably alter the interaction. For example, preliminary investigation shows that for the ZM interaction TWI solitons can appear in the pump wave even for the SFF case. This may provide an explanation for the numerically observed analogy between the FSF and SFF cases for the signal wave.

TWI-soliton theory explains the observed soliton features of the compression of the fastest wave. The inability to compress the intermediate speed pulse can be explained by the absence of TWI solitons in the corresponding envelope. Generally this nonsoliton wave has a very smooth distribution, with a duration approximately equal to the pump duration. Compression of the intermediate wave is not forbidden by TWI-soliton theory. In particular, it can appear as a byproduct of the compression of the fastest wave when the idler and signal speeds are close together, the behaviors of the two pulses are very similar, and it is possible to compress both pulses. In fact, compression of this sort was observed in a periodically poled lithium-niobate [27] experiment.

Although, the theory in the present paper describes only perfectly matched interaction, the generalization to nonzero phase mismatch is straightforward. The simple phase transformation in Ref. [11] show how phase mismatch is related to the real part of the eigenvalues λ_k. The effects of $\Delta k \neq 0$ will be considered in further publications.

ACKNOWLEDGMENTS

The research efforts of D.J.K. were supported in part by AFOSR and ONR. The research efforts of E.I. were supported in part by AFOSR.

APPENDIX A: DERIVATION OF EXPRESSIONS FOR PHASES

Analysis of the TWI equations on the basis of IST theory [17] shows that, when the envelopes of all three waves are separated, and on compact support, each of the waves corresponds to a certain scattering matrix:

$$S_1=\begin{pmatrix} 1 & 0 & 0 \\ 0 & \overline{a_1} & -\overline{b_1} \\ 0 & b_1 & a_1 \end{pmatrix}, \quad S_2=\begin{pmatrix} \overline{a_2} & -\overline{b_2} & 0 \\ b_2 & a_2 & 0 \\ 0 & 0 & 1 \end{pmatrix},$$

$$S_3=\begin{pmatrix} 1 & 0 & 0 \\ 0 & \overline{a_1} & -\overline{b_1} \\ 0 & b_1 & a_1 \end{pmatrix}, \tag{A1}$$

where λ_j are complex variables, $a_j=a_j(\lambda_j)$, $b_j=b_j(\lambda_j)$, $\overline{a_j}=\overline{a_j}(\lambda_j)$, and $\overline{b_j}=\overline{b_j}(\lambda_j)$ are analytic functions on the entire plane of the corresponding complex variables λ_j, and $\overline{a_j}(\lambda_j)=[a_j(\lambda_j^*)]^*$ and $\overline{b_j}(\lambda_j)=[b_j(\lambda_j^*)]^*$. Each of the three matrixes (A1) is called a Zakharov-Shabat matrix for the corresponding wave. Solitons in each envelope correspond to the zeros of the coefficient $a_j(\lambda_j)$ of the corresponding ZS matrix. In this paper, we will assume that the functions $a_j(\lambda_j)$ have zeros only at the points where λ_j is pure imaginary: $\lambda_j=i\eta_j$, where η_j is the imaginary part of λ_j. This situation corresponds to the case of perfect phase matching, $\Delta k=0$. Generalization to the case $\Delta k\neq 0$ can be done using the phase transformation from Ref. [11]. Here we do not do this for the sake of simplicity. Parameters η_j are connected by the relationships

$$\eta_1=\frac{\nu_{3,2}}{\nu_{2,1}}\eta_3=\alpha_1\eta_3, \tag{A2}$$

$$\eta_2=\frac{\nu_{3,1}}{\nu_{2,1}}\eta_3=\alpha_2\eta_3. \tag{A3}$$

Each of the functions $a_j(\eta_j)$ are assumed to have a finite number of zeros, $\eta_{j,k}$. The value of $\eta_{j,k}$ for which $a_j(\eta_{j,k})=0$ gives the amplitude of the kth soliton in the jth envelope. As described above, solitons can move from the pump to the signal and idler and back. When solitons change envelopes, their amplitudes must be normalized. If before the interaction the pump had n TWI solitons with amplitudes $\eta_{3,k}$, then after the interaction the signal and the idler waves will receive these solitons with their amplitudes dictated by the relationships

$$\eta_{1,k}=\frac{\nu_{3,2}}{\nu_{2,1}}\eta_{3,k}=\alpha_1\eta_{3,k}, \tag{A4}$$

$$\eta_{2,k}=\frac{\nu_{3,1}}{\nu_{2,1}}\eta_{3,k}=\alpha_2\eta_{3,k}. \tag{A5}$$

This means that if $a_3(\eta)$ in the beginning of the interaction has zeros at the points $\eta_{3,k}$, after the interaction, the elements $a_1(\eta)$ and $a_2(\eta)$ will have zeros at the points $\eta_{1,k}$ and $\eta_{2,k}$ connected with the pump solitons with the normalizations (A4) and (A5).

To find the final soliton phases, we need to obtain expressions of the ratios b_j/a_j for each wave at the end of the interaction. Such ratios in IST theory are called reflection coefficients. At each point where a_j becomes zero, b_j/a_j has a pole. Soliton phases $D_{j,k}$ can be obtained by taking residues of the reflection coefficients at those points where $a_j(\eta_{j,k})=0$. Such poles correspond to TWI solitons. (Here index j corresponds to the number of the envelope, and index k corresponds to the soliton number.) The overall scattering matrix S for the TWI problem is the product of the three matrixes corresponding to each of the interacting waves. If in the beginning of the interaction ($z\to-\infty, t\to-\infty$) the second wave was in the front of the third and the first wave followed the third, then

$$S^{(i)}=S_2^{(i)}S_3^{(i)}S_1^{(i)}, \tag{A6}$$

where the index i stands for ''initial.'' (Notice that our notations are different from that in Ref. [17].) Due to the differences between the speeds, the waves reorder after the interaction:

$$S^{(f)}=S_1^{(f)}S_3^{(f)}S_2^{(f)}, \tag{A7}$$

where an index f stands for ''final.'' The order of the final scattering matrices $S^{(f)}$ reflects the reordering of the pulses. The evolution of the elements $a_{n,m}$ of the scattering matrix S is given by the expression [17]

$$a_{n,m}(\lambda,z)=a_{n,m}(\lambda,0)\exp\left[-i\lambda z\left(\frac{v_m-v_n}{v_1v_2v_3}\right)\right], \tag{A8}$$

where v_i are the group speeds of the waves. Notice again, that in the present paper, the time and space coordinates are interchanged as compared with the work [17]. Expression (A8) enables us to relate the elements of the scattering matrix before and after the interaction. If in the beginning of the interaction, the wave with the smallest velocity v_2 was absent (the fastest wave with v_1 is the signal wave), then the corresponding ZS matrix for this wave is the identity matrix: $\bar{a}_2^{(i)}=a_2^{(i)}=1$ and $\bar{b}_2^{(i)}=b_2^{(i)}=0$. Equating $S^{(i)}$ and $S^{(f)}$ for this case, we obtain the expression for the reflection coefficient $\rho_2(\lambda)$ for the idler wave:

$$\frac{\bar{b}_2^{(f)}}{\bar{a}_2^{(f)}}=\frac{\bar{b}_3^{(i)}b_1^{(i)}}{\bar{a}_3^{(f)}\bar{a}_2^{(f)}}\exp\left[2\frac{\eta_2}{v_2}z\right]$$

or

$$\rho_2=\frac{b_2^{(f)}}{a_2^{(f)}}=\frac{b_3^{(i)}}{a_3^{(i)}}\bar{b}_1^{(i)}\exp\left[2\frac{\eta_2}{v_2}z\right]. \tag{A9}$$

Here we used the relationship $\bar{a}_2^{(f)}\bar{a}_3^{(f)}=\bar{a}_2^{(i)}\bar{a}_3^{(i)}$.

To obtain the final phases of the idler wave, one has to find the residues of the reflection coefficient (A9) at the points $\eta_{2,k}$ connected with the initial pump soliton amplitudes $\eta_{3,k}$ by relationships (A5):

$$D_{2,k}^{(f)}=\frac{-ib_3^{(i)}(\eta_3)}{\frac{d}{d\eta_2}a_3^{(i)}(\eta_3)\big|_{\eta_2=\eta_{2,k}}}\bar{b}_1^{(i)}\exp\left[2\frac{\eta_2}{v_2}z\right]$$

$$=\alpha_2D_{3,k}^{(i)}\bar{b}_1^{(i)}\exp\left[2\frac{\eta_2}{v_2}z\right]; \tag{A10}$$

when taking derivatives, we again used expression (A5).

The analogous expression for the reflection coefficient of the signal wave with the largest velocity v_1 cannot be obtained from Eqs. (A1)–(A7) directly. To find the reflection coefficients for this case, we use the fact that if $A_j(t,z)$ are solutions of system (1), then the functions $-A_j(-t,-z)$ are also solutions of the same system. The final result of the direct problem will serve as initial conditions for the problem inverted in time and space, and vice versa. Therefore we will consider a process where, at the end of the interaction, a small signal wave $A_1(t)$ with a speed v_1 is in the front of a large pump wave $A_3(t)$ with no idler wave. The initial conditions for this reversed process will be a signal wave with the amplitude $A_1(-t)$ chasing a large pump with the amplitude $A_3(-t)$ with no idler wave. The final coefficients a and b for such an inverted process will be equal to the initial values of the direct process, and vice versa. Using this fact, we obtain

$$\frac{b_1^{(f)}}{a_1^{(f)}}=\frac{b_1^{(i)}}{a_1^{(i)}a_3^{(i)}}\exp\left[2\frac{\eta_{1,k}}{v_1}z\right]. \tag{A11}$$

The final soliton phases can be obtained by taking residues of the functions (A9) and (A11) at the points where coefficients a and $\bar{a}$ of the corresponding ZS matrices are equal to zero:

$$D_{1,k}^{(f)}=\frac{b_1^{(i)}(\eta_1)}{a_1^{(i)}\dfrac{d}{d\eta_1}[a_3^{(i)}(\eta_3)]\big|_{\eta_1=\eta_{1,k}}}\exp\left[-2\frac{\eta_{1,k}}{v_1}z\right]. \tag{A12}$$

Notice that the differentiation here is done with respect to the variable η_1, but that the coefficient $a_3(\eta_3)$ is a function of η_3. The connection between η_1 and η_3 is given by relations (A4) and (A5). Expression (4) shows that an intense pump wave consist almost entirely of TWI solitons. In the following analysis, we will assume that the pump before the interaction consisted only of TWI solitons and had no radiation. In this case the coefficients $a_3(\eta)$ can be written as

$$a_3(\eta_3)=\prod_{k=1}^{n}\frac{\eta_3-\eta_{3,k}}{\eta_3+\eta_{3,k}}, \tag{A13}$$

where $\eta_{3,k}$ is as usual the amplitude of the kth soliton in the pump. Differentiating Eq. (A13) with respect to η_1 and using relationship (A2) we obtain

$$\frac{d}{d\eta_1}\left[\prod_{j=1}^{n}\frac{\eta_3-\eta_{3,j}}{\eta_3+\eta_{3,j}}\right]\Bigg|_{\eta_1=\eta_{1,k}}=\frac{1}{\alpha_1}\frac{d}{d\eta_3}\left[\prod_{k=1}^{n}\frac{\eta_3-\eta_{3,j}}{\eta_3+\eta_{3,j}}\right]\Bigg|_{\eta_3=\eta_{3,k}}=\frac{1}{2\alpha_1\eta_{3,k}}\prod_{\substack{j=1\\ j\neq k}}^{n}\frac{\eta_{3,k}-\eta_{3,j}}{\eta_{3,k}+\eta_{3,j}}. \tag{A14}$$

Notice that the derivative of the product in Eq. (A14) has only one nonzero term at the points $\eta_3=\eta_{3,k}$. After a substitution of Eq. (A14) into expression (A12), we obtain the expression for the final phases of the signal wave:

$$D_{1,k}^{(f)}=\left(\frac{b_1^{(i)}}{a_1^{(i)}}\right)2\alpha_1\eta_{3,k}\prod_{\substack{j=1\\ j\neq k}}^{n}\frac{\eta_{3,k}+\eta_{3,j}}{\eta_{3,k}-\eta_{3,j}}\exp\left[2\frac{\eta_{1,k}}{v_1}z\right]. \tag{A15}$$

One should be careful when using expression (A15). Because this formula was obtained by reversing time, the output shape of the signal wave determined by Eq. (A15) will also be reversed in time.

APPENDIX B: ZAKHAROV-SHABAT PROBLEM AND REFLECTION COEFFICIENTS

Expressions (A10) and (A15) connect the initial and final scattering data for the parametric amplification process. Both expressions contain parameters a and b from Zakharov-Shabat scattering matrixes (A1). In this appendix we show the connection between these coefficients and the initial data.

The connection is based on the direct ZM scattering problem [17] scattering problem. When the pulses are physically separated, as they are before the interaction, the ZM scattering problem reduces to a set of three (one for each pulse) ZS scattering problems

$$\begin{aligned} u_i'+i\lambda u_i&=q_i(t)v_i,\\ v_i'-i\lambda v_i&=-q_i^*(t)u_i, \end{aligned} \tag{B1}$$

with potential $q_i(t)$ given by

$$q_i(t)=\frac{1}{\gamma_i}A_{i,0}^*(t). \tag{B2}$$

The functions u and v are the eigenfunctions and the parameters λ the eigenvalues of the ZS problem (B1).

If potential (B2) decreases sufficiently rapidly as $t\to\pm\infty$ that

$$\int_{-\infty}^{\infty}|q_i(t)|e^{k|t|}dt<\infty \tag{B3}$$

for any positive number k, then all solutions of system (B1) are asymptotic as $t\to\pm\infty$ to simple exponential functions. (Clearly, this assumption imposes no physical restrictions on the pulses that can be considered since all optical pulses are bounded in both time and space.) Moreover, any solution of Eq. (B1) can be written either as a linear combination of the two solutions ϕ and $\overline{\phi}$ system (B1) satisfying

$$\phi\to\begin{bmatrix}1\\0\end{bmatrix}e^{-i\lambda t},\quad \overline{\phi}\to\begin{bmatrix}0\\-1\end{bmatrix}e^{i\lambda t}\quad \text{when } t\to-\infty, \tag{B4}$$

or as linear combinations of the two solutions ψ and $\overline{\psi}$ satisfying

$$\psi\to\begin{bmatrix}0\\1\end{bmatrix}e^{i\lambda t},\quad \overline{\psi}\to\begin{bmatrix}1\\0\end{bmatrix}e^{-i\lambda t}\quad \text{when } t\to+\infty, \tag{B5}$$

where we have omitted the index i for clarity. Either pair of functions forms a complete set of solutions of the system (B1). So the first pair of solutions (B4) are a linear combination of the the second pair (B5), i.e.,

$$\begin{aligned} \phi&=a\overline{\psi}+b\psi\to\begin{pmatrix}a & e^{-i\lambda t}\\ b & e^{i\lambda t}\end{pmatrix}\quad \text{as } t\to+\infty,\\ \overline{\phi}&=\overline{b}\psi-\overline{a}\psi\to\begin{pmatrix}\overline{b} & e^{-i\lambda t}\\ -\overline{a} & e^{i\lambda t}\end{pmatrix}\quad \text{as } t\to+\infty. \end{aligned} \tag{B6}$$

The coefficients a, b, $\overline{a}$, and $\overline{b}$ (which depend upon the spectral parameter λ) relating the two sets of solutions form the Zakharov-Shabat scattering matrix

$$S_{ZS}=\begin{pmatrix}a(\lambda), & -\overline{b}(\lambda)\\ b(\lambda), & \overline{a}(\lambda)\end{pmatrix}. \tag{B7}$$

In Ref. [23] it was shown that for potentials satisfying (B3) $a(\lambda)$ and $\overline{a}(\lambda)$ are analytic in the upper-half and lower-half complex planes, respectively. Formulas (5)–(7) show how to

recreate the shape of the pulse with known soliton content (and negligible radiation). System (B1) shows how to compute the soliton spectrum and radiation content of the initial pulses $A_{i,0}(t)=\gamma_i q_i(t)$. The radiation spectrum in $q_i(t)$ is determined by the definition (B6) of the scattering matrix and the solutions of system (B1) and boundary conditions (B4) and (B5).

To complete our analysis we derive simple approximations, in terms of the initial pulse profiles, for the values of $\overline{b_1}$ and $b_1^{(i)}/a_1^{(i)}$ occurring in (A10) and (A15). To do this we need the ZS scattering matrix (B7) for the small potential $q(t)=A_{1,0}(t)/\gamma_1$ corresponding to the small initial signal pulse at the purely complex values $\lambda=i\eta_{1,k}=i\alpha\eta_{3,k}$ corresponding to the solitons in the intense initial pump. As before, we restrict attention to potentials $q(t)=q^*(t)$, i.e., without a phase modulation. Since the potential $q(t)$ is very small we employ a perturbation expansion. Assuming the potential q is of order ϵ and substituting the expansions

$$u(t)=u_0+\epsilon u_1(t)+\epsilon^2 u_2(t)+\cdots,$$
$$v(t)=v_0+\epsilon v_1(t)+\epsilon^2 v_2(t)+\cdots,$$

and $\lambda=i\eta$ into system (B1), and equating coefficients gives the zeroth-order equations

$$u_0'-\eta u_0=0,$$
$$v_0'+\eta v_0=0,$$

with solutions (B8)

$$u_0=e^{\eta t},$$
$$v_0=e^{-\eta t}.$$

Note that in Eq. (B8) and what follows the subscript refers to the order of the approximation. Substituting into Eq. (B1) gives the first-order system

$$u_1'-\eta u_1=q_1(t)e^{-\eta t},$$
$$v_1'+\eta v_1=-q_1(t)e^{\eta t}. \tag{B9}$$

For the boundary conditions (B4), from Eq. (B9) we obtain

$$u(t)\approx e^{\eta t}\left[\int_{-\infty}^{t} q(t)e^{-2\eta t}dt+1\right],$$
$$v(t)\approx -e^{-\eta t}\int_{-\infty}^{t} q(t)e^{2\eta t}dt, \tag{B10}$$

which with Eq. (B6) immediately gives

$$a(\eta_k)\approx 1+\int_{-\infty}^{\infty} q(t)e^{-2\eta_k t}dt\approx 1,$$
$$b(\eta_k)\approx -\int_{-\infty}^{\infty} q(t)e^{2\eta_k t}dt. \tag{B11}$$

Computing $\overline{a}$ and $\overline{b}$ is similar. Solving Eq. (B9) for the initial conditions (B4) gives

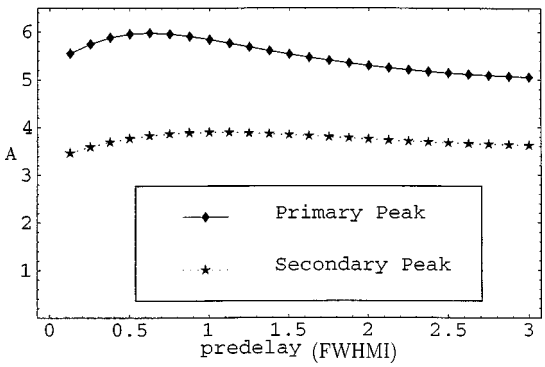

FIG. 12. Effect of predelay on interaction. Signal output amplitude for the interaction of an intense—4 sech(t)—pump with a small—0.1 sech[3($t+\Delta t$)]—trigger pulse for predelays Δt of the small trigger ranging from 0.125 FWHMI (of the large pump) to 3 FWHMI.

$$u(t)\approx e^{\eta t}\int_{-\infty}^{t} q(t)e^{-2\eta t}dt,$$
$$v(t)\approx -e^{-\eta t}\left[\int_{-\infty}^{t} q(t)e^{2\eta t}dt+1\right]. \tag{B12}$$

Substituting into Eqs. (B6) and (B12) gives $\overline{a}$ and $\overline{b}$ as

$$\overline{a}(\eta_k)\approx 1+\int_{-\infty}^{\infty} q(t)e^{2\eta_k t}dt\approx 1$$
$$\overline{b}(\eta_k)\approx \int_{-\infty}^{\infty} q(t)e^{-2\eta_k t}dt. \tag{B13}$$

Expressions (A10), (A15), (B11), and (B13) give formula (18). Before using (B1) the function $q(t)$ must be reversed in time and the coordinate t must be changed to $-t$.

APPENDIX C: NUMERICAL QUANTIFICATION OF EFFECT OF PREDELAY

Numerous numerical simulations were run in order to validate the use of the simpler ZS analysis for the FSF problem. The issue here is when can pulses be considered well seperated. Figure 12 summarizes the signal output from a sequence of numerical simulations of the decay of an intense four soliton [4 sech(t)] pump pulse triggered by a small [0.1 sech(3($t+\Delta t$))] trigger pulse for a range of values—in units of the FWHMI of the pump—of the predelay Δt. For predelays ranging from 0.125–3 FWHMI of the pump the signal output had the characteristic alternating soliton profile illustrated in Fig. 3: in Fig. 12, ''Primary Peak'' indicates the amplitude of the largest soliton, while ''Secondary Peak'' indicates the amplitude of the next largest soliton. The results indicate that for small trigger pulses and predelays greater than 0.125 FWHMI (of the intense pump) the ZS analysis gives less than a 15% error in the amplitude of the leading soliton.

[1] S. A. Akhmanov, A. S. Chirkin, K. N. Drabovich, A. I. Kovrigin, R. V. Khohlov, and A. P. Sukhorukov, IEEE J. Quantum Electron. **QE-4**, 588 (1968).

[2] Y. Wang and R. Dragila, Phys. Rev. A **41**, 5645 (1990).
[3] A. Stabinis, G. Valiulis, and E. A. Ibragimov, Opt. Commun. **86**, 301 (1991).
[4] Y. Wang and B. Luther-Davies, Opt. Lett. **17**, 1459 (1992).
[5] C. Y. Chien, G. Korn, J. S. Coe, J. Squier, G. Mourou, and R. S. Craxton, Opt. Lett. **20**, 353 (1994).
[6] J. D. V. Khaydarov, J. H. Andrews, and K. D. Singer, Opt. Lett. **19**, 831 (1994).
[7] J. D. V. Khaydarov, J. H. Andrews, and K. D. Singer, J. Opt. Soc. Am. B **12**, 2199 (1995).
[8] A. Umbrasas, J. C. Diels, J. Jacob, and A. Piskarskas, Opt. Lett. **19**, 1753 (1994).
[9] S. Fournier, R. Lopez-Martens, C. Le Blank, E. Baubeau, and F. Salin, Opt. Lett. **23**, 627 (1998).
[10] E. Ibragimov and A. Struthers, Opt. Lett. **21**, 1582 (1996).
[11] E. Ibragimov and A. Struthers, J. Opt. Soc. Am. B **14**, 1472 (1997).
[12] V. E. Zakharov and S. V. Manakov, Zh. Eksp. Teor. Fiz. **69**, 1654 (1975) [Sov. Phys. JETP **42**, 842 (1975)].
[13] D. J. Kaup, Stud. Appl. Math. **55**, 9 (1976).
[14] L. Torner, C. Menyuk, and G. Stegeman, J. Opt. Soc. Am. B **12**, 889 (1995).
[15] A. V. Buryak, Y. S. Kivshar, and S. Trillo, Opt. Lett. **20**, 1961 (1995).
[16] E. Ibragimov, J. Opt. Soc. Am. B **15**, 97 (1998).
[17] D. J. Kaup, A. Reiman, and A. Bers, Rev. Mod. Phys. **51**, 275 (1979).
[18] Yu. N. Karamzin and A. P. Sukhorukov, Pis'ma Zh. Eksp. Teor. Fiz. **20**, 734 (1974) [JETP Lett. **20**, 339 (1974)].
[19] E. Ibragimov, J. D. Khaydarov, K. D. Singer, and Allan Struthers, in *Conference on Lasers and Electro-Optics*, Vol. 11 of OSA Technical Digest Series (Optical Society of America, Washington, DC, 1997), pp. 200 and 201.
[20] M. J. Ablowitz and P. A. Clarkson, *Solitons, Nonlinear Evolution Equations and Inverse Scattering* (Cambridge University Press, Cambridge, 1991).
[21] D. J. Kaup, Phys. Rev. A **16**, 704 (1977).
[22] J. W. Miles, SIAM (Soc. Ind. Appl. Math.) J. Appl. Math. **41**, 2 (1981); **41**, 227 (1981).
[23] M. J. Ablowitz, D. J. Kaup, A. C. Newell, and H. Segur, Stud. Appl. Math. **53**, 249 (1974).
[24] H. A. Haus and M. N. Islam, IEEE J. Quantum Electron. **QE-21**, 1172 (1985).
[25] E. Ibragimov, A. Struthers, and D. J. Kaup, Opt. Commun. **152**, 101 (1998).
[26] V. G. Dmitriev, G. G. Gurzadyan, and D. N. Nikogosyan, *Handbook of Nonlinear Optical Crystals* (Springer-Verlag, Berlin, 1997).
[27] S. D. Butterworth, L. Lefort, and D. C. Hanna (private communication).